Food Hydrocolloids 140 (2023) 108625

Contents lists available at ScienceDirect

Food Hydrocolloids

journal homepage: www.elsevier.com/locate/foodhyd

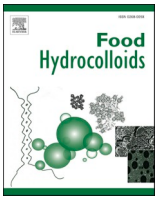

Electrosprayed microparticles from inulin and poly(vinyl) alcohol for colon targeted delivery of prebiotics

Keara T. Saud [a,b,*,1], Jin Xu [b,c,1], Sabina Wilkanowicz [d], Yue He [b,c], James J. Moon [b,c,e,f], Michael J. Solomon [e,f]

[a] Department of Materials Science and Engineering, University of Michigan, Ann Arbor, MI, USA
[b] Biointerfaces Institute, University of Michigan, Ann Arbor, MI, USA
[c] Department of Pharmaceutical Sciences, University of Michigan, Ann Arbor, MI, USA
[d] Warsaw University of Technology, Faculty of Civil Engineering, Mechanics and Petrochemistry, Institute of Chemistry, Płock, Poland
[e] Department of Biomedical Engineering, University of Michigan, Ann Arbor, MI, USA
[f] Department of Chemical Engineering, University of Michigan, Ann Arbor, MI, USA

A B S T R A C T

Recent studies have highlighted the prebiotic effect of inulin through the selective promotion of colon-residing bacteria, modulation of the composition of the gut microbiome, and consequent generation of beneficial effects on gastrointestinal inflammation, diabetes, and cancer. However, as a water-soluble polysaccharide, the prebiotic effect of inulin is limited by low delivery efficiency and short retention time within the colon. In this study, inulin microparticles (MPs) were produced by the electrospray method, and their material properties and bioavailability were evaluated. Inulin was electrosprayed with poly(vinyl) alcohol (PVA) (MW = 89,000–98,000 g/mol) to improve its processability and mucoadhesive properties. MPs produced at PVA:Inulin mass ratio 1:3 were of diameter 0.42 ± 0.46 μm. FTIR and confocal laser scanning microscopy confirmed the presence and colocalization of the PVA and inulin in the particles. MP suspensions exhibited a time dependent viscoelastic rheological response that trended with time toward the response of the inulin suspension. Additionally, MP suspensions exhibited greater viscosity and shear thinning behavior than their individual components and two-component mixtures. The gut retention of inulin in mice was prolonged when delivered in these MP suspensions relative to inulin suspensions and PVA-inulin two-component mixtures. The increased retention is hypothesized to be a result of the effect of PVA on rheological and mucoadhesive properties. The increased retention of inulin leads to improved availability of inulin for gut microbiota which can support applications in drug delivery and foods.

1. Introduction

Inulin is a fructan polysaccharide that occurs naturally in many foods, such as leeks, asparagus, onion, garlic, and chicory (Carlson et al., 2018). It is commonly used in the food industry to replace sugar or fat and to modify rheological properties (Barclay et al., 2010; Liu et al., 2022; Mensink et al., 2015; Nieto-Nieto et al., 2015; Zhang et al., 2019). Inulin is a dietary fiber that is not digested in the stomach and small intestine but instead is metabolized by commensal bacteria in the colon. Consuming prebiotics such as inulin has been associated with a number of health benefits, including stimulation of the immune system, production of beneficial metabolites, and reduced allergy risks (Carlson et al., 2018; Kolida et al., 2002; Van De Wiele et al., 2007; Wahbi et al., 2020).

Recent studies have combined inulin with PVA and plasticizers to expand its application and to make functional biomaterials with enhanced mechanical properties (Kim et al., 2020; Youn et al., 2019). UV treatment with plasticizers has greatly improved the physical properties of inulin while maintaining its biodegradability and antimicrobial activities (Youn et al., 2019). The same UV curing method has been additionally used to create biomaterials that could serve as transdermal drug delivery systems (Kim et al., 2020). These studies show the good compatibility between inulin and PVA as well as the versatility of this combination as a biomaterial. Nevertheless, the aforementioned studies only focused on *ex vivo* applications and have not expanded to the prebiotic effects and human health.

Concerning human health, studies have suggested that the formulation of inulin affects its prebiotic efficacy. Specifically, when administered in a gel form, inulin exerts a synergistic effect (compared to inulin suspensions) with immune checkpoint blockade therapy in various murine tumor models (Han et al., 2021). The effect is generated through modulation of the gut commensal microorganisms and was

* Corresponding author. Department of Materials Science and Engineering, University of Michigan, Ann Arbor, MI, USA
E-mail address: ktsaud@umich.edu (K.T. Saud).
[1] These people contributed equally to this work.

https://doi.org/10.1016/j.foodhyd.2023.108625
Received 7 November 2022; Received in revised form 18 February 2023; Accepted 22 February 2023
Available online 23 February 2023

explained by the increased inulin retention in the colon when gelled and the resulting increased probiotic bacteria and short-chain fatty acid (SCFA) production (Han et al., 2021). Wahbi et al. also show that the formulation of inulin affects its properties (Wahbi et al., 2020). They electrospun inulin into composite nanofibers with polyvinyl alcohol (PVA) and found that the nanofibers increased the prebiotic activity by 38% compared to their suspension counterparts. Here inulin suspensions, inulin gels, and inulin nanofibers primarily differ in their physical forms: specifically, the microstructure and surface area-to-volume ratios of these materials vary. Inulin suspensions lack any network microstructure and have a small surface area-to-volume ratio relative to nanosized samples. In contrast, inulin gels have a microstructure responsible for their modified and more solid-like rheological properties; and inulin nanofibers have a much larger surface area to volume ratio.

In addition to gel, nanofiber, and suspension formulations, inulin can also be made into microparticles (MPs) via several techniques, including electrospraying, spray drying, and solvent-precipitation (Beirão-da-Costa et al., 2013; Jain et al., 2014; Sarkar et al., 2018; Zaeim et al., 2019). Inulin in particle form has been studied for targeting the colon (Jain et al., 2014; Zaeim et al., 2019). This form has additionally been studied for the encapsulation of bioactive molecules as well as in conjunction with bioactive molecules to improve molecule stability and viability (Afinjuomo et al., 2021; Beirão-da-Costa et al., 2013; Zaeim et al., 2020). However, how this particle form affects inulin's gut retention properties has not been the subject of systematic study.

The first part of this paper describes the creation and characterization of the material properties of inulin MPs; the second part examines inulin gut retention *in vivo* when delivered as a MP formulation. The MPs are prepared via electrospraying inulin and PVA. Electrospraying is a form of electrohydrodynamic processing (EHDP) that utilizes a high potential difference between a polymer solution and a collector plate to yield particle or capsule production. The high potential difference and the dominance of the solution's surface tension over the electrostatic repulsion cause the formation of nano- and micro-particles. The advantages of this technique over others include its low cost, its scalability, its reproducibility, and its benign processing conditions (i.e., ambient temperatures and pressures). Because inulin is not electrosprayable as a pure component (Jain et al., 2014), inulin has been blended with PVA for successful spraying. PVA is biocompatible, of low toxicity, and used in FDA-approved medical products. It additionally exhibits mucoadhesive properties when highly hydrolyzed (Popov et al., 2016) and readily dissolves in solvents that are non-hazardous. It is also well-studied and commonly used for electrospraying, including with inulin (Felice et al., 2015; Ghorani & Tucker, 2015; Jacobsen et al., 2018; Oguz et al., 2018; Rostami et al., 2019; Wahbi et al., 2020). To simulate the oral dosage form for *in vivo* studies in mice, the resulting inulin MPs are characterized in the following ways: 1) morphology and size distribution in dry and hydrated states; 2) chemical composition and the localization of these components; 3) transient and steady-state rheology when suspended in water, and 4) inulin release profile. We correlate these properties with the results of inulin gut retention studies *in vivo* to better understand bioavailability in the gut.

2. Experimental section

2.1. Materials

PVA (Mw = 89,000–98,000 g/mol, 99% hydrolyzed), inulin from chicory, FITC-inulin, ethanol, glacial acetic acid (AA), and fluorescein isothiocyanate (FITC) were purchased from Sigma Aldrich (St. Louis, MO, USA). Cyanine5 (Cy5) and Cyanine7 (Cy7) amines were purchased from Lumiprobe (Cockeysville, MD, USA). The fructan assay kit was from Megazyme (Ireland).

2.2. Fluorescence conjugation of inulin and PVA

PVA was labeled with FITC following the procedure published by (Kaneo et al., 2005). Briefly, PVA (2.5 g) was dissolved in DMSO (66.6 mL) and pyridine (416.6 μL) under stirring at 80 °C for 24 h. FITC (83 mg) and dibutyltin dilaurate (31 μL) were added to the PVA solution, and the reaction was carried out for 2 h at 95 °C in darkness. The crude product was precipitated and washed with IPA, followed by dialysis against DEMI water and lyophilization.

Cy5-inulin or Cy7-inulin conjugates were synthesized using the method described by (Hauser-Kawaguchi et al., 2019). In brief, Carboxymethyl inulin (CMI) was first produced by dissolving 500 mg inulin in 2 M NaOH, added with 276 mg chloroacetic acid, and heating to 70 °C for 75 min. The solution was neutralized with acetic acid after cooling, and CMI was precipitated by cold ethanol. Resulted CMI (40-50 mg) was activated in 10 mL 1 M equivalent of NHS and EDC for 1.5 h. The activated CMI solution was subsequently added dropwise to Cy5/Cy7-amine (Lumiprobe) (10–15 mg, 12.2–18.3 μM), dissolved in dimethyl sulfoxide (DMSO). The conjugation of the dye to CMI was allowed to proceed for 24 h at room temperature, in the dark with shaking. Dialysis was carried out (Float-a-Lyzer, Spectrum Labs, Phoenix, AZ) against water, and the resulted solution was lyophilized until dry powders was obtained.

2.3. Preparation of mixtures for electrospraying

A stock solution of 5.0 wt% PVA was weighed and dissolved in a solution containing 84 vol% H_2O, 6 vol% AA, and 10 vol% ethanol (84/6/10 H_2O/AA/ethanol) (Felice et al., 2015). The stock solution was left to fully dissolve in a 70 °C oven overnight. Inulin suspensions made with 15 wt% inulin in ultrapure H_2O (18.2 MΩ-cm) were prepared and left in a 40 °C water bath for 20 min. This concentration of inulin was chosen to maximize the inulin content but avoid inulin gelation that can occur with higher inulin concentrations (Han et al., 2021). For confocal laser scanning microscopy (CLSM) and IVIS imaging (described below), PVA solutions and inulin suspensions were prepared by adding FITC-PVA and Cy7-inulin in the ratios of 1:9 and 1:19 to the unconjugated forms, respectively.

Following dissolution, equal parts PVA solution and inulin suspension were combined, resulting in a final mixture concentration of 2.5 wt % PVA and 7.5 wt% inulin in H_2O/AA/Ethanol (91/3.4/5.6 by volume, shifted slightly because the inulin suspension was only in water for this case (Felice et al., 2015)). This was the minimum concentration of PVA that resulted in sustained, successful MP production. Preliminary studies showed that sustained fiber production (electrospinning) could also occur with inulin when solutions contained only water. PVA concentrations were increased to a final concentration of 7.5 wt%, and final inulin concentrations remained constant at 7.5 wt%.

For pure PVA particles, minimizing PVA content was not a goal, so 6.0 wt% PVA in H_2O/AA/Ethanol (84/6/10 by volume) (Felice et al., 2015) was combined with equal parts ultrapure water. This resulted in a final concentration of 3.0 wt% PVA in H_2O/AA/Ethanol (91/3.4/5.6 by volume). A higher PVA concentration allowed for a greater particle production rate while maintaining stable electrospraying. Each newly combined sample was well mixed before further characterization or used in EHDP.

2.4. Characterization of mixtures for electrospraying

The conductivity of PVA solutions and PVA-inulin mixtures used for electrospraying was measured using a compact conductivity meter (EC 11, Horiba, Japan). Rheological properties were measured using an Anton Paar MCR 702 rheometer (Austria) at 20 °C. PVA solutions were measured in a cone and plate configuration ($\theta = 2°$, 50 mm in diameter). PVA-inulin mixtures were measured in a parallel plate configuration (50 mm in diameter) with 600-grit sandpaper adhered to the rheometer

tooling to mitigate any potential for wall slip. The viscosity is measured and reported at the high shear limit of $\dot{\gamma} = 100\ s^{-1}$ (Librán et al., 2017; Perez-Masia et al., 2014). Data points were log spaced. Measurements at a given shear rate were performed until the viscosity was constant with an allowance of 1%, and the signal was averaged for the last 0.5 s. PVA-inulin mixtures were allowed to rest quiescently for 1 h prior to measurement to achieve a steady state (SI Fig. 1). The surface tension of the prepared mixtures was measured using an optical goniometer (Rame-hart Instrument Co., New Jersey, USA, Drop Image Advanced software). All measurements were performed in triplicate at a minimum.

2.5. Microparticle production via electrospraying

The EHDP equipment was assembled in a horizontal configuration with a high-voltage power supply (P030HP2M, Acopian, USA) and a digital syringe pump (KDS100, KD Scientific, Massachusetts, USA). This equipment is contained in a covered plastic box to reduce photobleaching and minimize changes in relative humidity. After the polymeric mixture was prepared, it was loaded into a disposable syringe (Becton Dickinson, New Jersey, USA) with an 18-gauge stainless steel needle. The syringe was attached to the pump so that the tip-to-collector distance was approximately 12 cm. The steel collector plate is 28 cm × 28 cm and is covered with standard aluminum foil. The needle is attached to one electrode, and the collector plate is attached to the other electrode. The pump is set to a flow rate of 0.5 mL/h for PVA-inulin mixtures, 0.4 mL/h for fluorescently labeled PVA-inulin mixtures, and 0.4 mL/h for pure-PVA solutions. The voltage was adjusted between 21 and 25 kV to achieve a stable Taylor cone. The collection time varied between 3 and 18 h to produce adequate amounts of samples for testing. Approximately 50 wt% of the sample was recoverable and useable after each process, as assessed using scanning electron microscopy. These electrospraying conditions were chosen to maximize particle production rather than to compare electrosprayability. Particle properties were then compared by means of the characterization techniques discussed in the methods.

2.6. Characterization of MP powder

2.6.1. Morphological characterization of MPs

Scanning electron microscopy (SEM; Tescan MIRA3, Pennsylvania, USA) was used to characterize the size and morphology of electrosprayed MPs. Specimens were sputter-coated with gold. An operating voltage of 5 kV and an average working distance of 9.7 mm were used. Images for morphological analysis of dry MPs were captured at 35 kx magnification. Images for size analysis of dry MPs were captured at 20kx magnification. Particle size analysis of the electrosprayed inulin-PVA MPs was performed by measuring the particle diameter with ImageJ. If the particle was not perfectly spherical, the largest diameter measurement was taken. The particle size dispersity was compared using the coefficient of variation, $Cv = \sigma/\mu$, where σ is the standard deviation and μ is the average particle size (Felice et al., 2015). In all cases, a minimum of 900 particles from three random parts of the sample were analyzed to determine size distributions.

2.6.2. Hydrated size distribution

A Malvern Mastersizer 2000 with Hydro 2000S wet dispersion unit (United Kingdom) was used to measure the hydrated particle size distribution of the MPs. Samples were dispersed in water with equivalent inulin concentrations of 180 mg/mL and gently mixed. After 30min, samples were added to the chamber, with the stirring speed at 1750 rpm and sonication. Data were analyzed using the following parameters: particle refractive index was set to 1.50, the dispersant was taken as pure water, and obscuration was controlled in the range of 2–15%.

2.6.3. Fourier transform infrared (FTIR) spectroscopy

FTIR spectroscopy (Jasco FTIR-4100, Japan) was used for chemical composition analysis and comparison of the prepared MPs with their pure components. Samples were prepared by filling the instrument well with powders of pure PVA, pure inulin, or PVA-inulin MPs. Spectra were collected with 1 cm-1 resolution and an average of 64 scans over a spectral range of 4000–500 cm-1. Spectra were normalized and examined by Spectra Manager software.

2.6.4. Confocal laser scanning microscopy (CLSM)

An inverted confocal laser-scanning microscope (CLSM) (Nikon A1Rsi equipped with NA = 1.4×, 100× objective, Japan) was used to examine the dry and hydrated MPs as well as the hydrated inulin suspension. The MPs to be imaged were prepared with FITC-PVA and Cy5-inulin, as described in sections 2.3 and 2.5. The inulin suspensions to be imaged were prepared with FITC-inulin (Sigma Aldrich) at a ratio of 1:9 to the unconjugated form of inulin. The following two channels were used: the Cy5-inulin was imaged with a 641 nm excitation and an emission band from 663 to 738 nm, and the FITC-PVA and FITC-inulin were imaged with a 488 nm excitation and an emission band from 500 to 550 nm.

Samples of dry PVA-inulin MPs were imaged in an 8-well plate (Thermo Fisher Scientific). For studies of hydration kinetics, inulin as-received or PVA-inulin MPs were suspended in ultrapure water at a concentration equivalent to those used in the rheological characterization, as described in section 2.8. Specifically, 180 mg/mL and 240 mg/mL were used, respectively. After combining the material with water, samples were vortexed mixed briefly for homogeneity. Immediately following, they were added to their respective imaging containers and mounted onto the microscope. Inulin suspensions were imaged in a sealed 8-well plate and PVA-inulin MP suspensions were imaged in a smaller device to conserve sample. The smaller device was made with a silicone spacer (1 mm thick and 4.5 mm in diameter, Grace Biolabs) adhered on a glass slide and sealed. Images were taken at approximately t = 0 s, 1800 s, 3600 s, 7200 s, and 14,400 s at a constant height of 5 μm above the coverslip. Swelling, aggregation, and any evolution with time were examined.

2.7. Inulin release study

120 mg PVA-inulin MPs were weighed and dispersed in 5 mL simulated intestinal fluid (SIF without Pancreatin, USP 26). The dispersion was incubated at 37 °C, 400 rpm and 100 μL samples were collected at the desired time point with 100 μL fresh buffer replenished immediately. Samples were centrifuged at 20,000 g for 5 min to remove undissolved particles. Supernatants were collected, and inulin concentration was measured by the Fructan Assay Kit (Megazyme, K-FRUC); readouts were acquired by the plate reader (Biotek Synergy NEO 2, USA).

2.8. Rheological characterization of MP suspensions and PVA-inulin mixtures

Characterization of the transient and steady-state rheology of PVA-inulin MP suspensions was performed and compared to that of four controls: PVA MP suspensions, PVA solutions, inulin suspensions, and two-component mixtures all made with equivalent concentrations of PVA and inulin. All samples were prepared to match gut retention studies, as described in section 2.9. Briefly, MPs and control mixtures were prepared in ultrapure water at a fixed concentration of 180 mg/mL inulin and 60 mg/mL PVA. For PVA-inulin MPs, this corresponded to 240 mg MP/mL. For PVA MPs, this corresponded to 60 mg/mL. For inulin suspensions, this corresponded to 180 mg/mL of inulin. For PVA solutions, preparation was conducted by dissolving PVA in water (60 mg/mL) at 70 °C. For the two-component mixture, the following was performed: first, the required amount of PVA (60 mg/mL PVA) was dissolved in water at 70 °C. Then the required amount of inulin (180 mg/mL) was added to the PVA solution. After preparation, all samples were well vortexed and left in a 37 °C water bath for 30 min to fully

disperse either the MPs, the inulin, the PVA, or the two-component mixture. Samples were allowed to rest at room temperature for approximately 10 min before loading in the rheometer.

An Anton Paar MCR 702 rheometer (Austria) was used with Peltier temperature-controlled plate and hood at 20 °C. A smooth 50 mm cone and plate geometry ($\theta = 2°$) was used for PVA solutions. A 25 mm and 50 mm parallel plate geometry was used for MP suspensions and two-component mixtures, respectively. Sandpaper (600 grit) was adhered to the parallel plate fixtures to address wall slip and a solvent trap was used to minimize sample evaporation. A study of the effect of gap at h = 500, 750, and 1000 μm was performed with the PVA-inulin MPs; it revealed no gap dependence in the rheological properties (SI Fig. 3). A 500 μm gap was used for all rheological measurements.

We measured the time-dependent linear viscoelastic moduli ($\omega = 1$ rad/s, $\gamma = 0.04\%$) of samples for a duration of 4 h (SI Fig. 2 shows linear regime). Following these 4-h time sweeps, two additional rheological tests were performed. First, the frequency-dependent linear viscoelastic moduli were measured from $\omega = 0.1$–100 rad/s ($\gamma = 0.04\%$). Next, the steady-state viscosity was measured as a function of shear rate over the range of 0.1–300 s^{-1}. Data points were log spaced. To achieve steady-state, measurements at a given shear rate were performed until the viscosity was constant with an allowance of 1% and the signal was averaged for the last 0.5 s. All data is collected with at least 3 replicates.

2.9. Gut retention studies

For the *in vivo* imaging of gut retention, Cy-7 labeled inulin was added in the PVA-inulin MPs as described in section 2.3 or was added to inulin suspensions in 1:19 for the other control groups. MPs, inulin, and PVA-inulin mixtures were orally administered to BALB/c mice at the dose of 36 mg inulin per mouse, five mice in each group, and images were taken every 2 h under anesthesia. Fecal pellets were collected every 2.5 h. Images were acquired and analyzed using IVIS Lumina Living Image Software (v.4.5.5).

For fecal inulin quantification, mice were fed on alfalfa-free diet (AIN-93 M) 24 h before the experiment to minimize interference of fructose derived from food. Then PVA-inulin MPs and equal amounts of inulin or inulin with PVA were suspended in water and administered to BALB/c mice by oral gavage. Fecal pellets were collected every 2.5 h and homogenized in water. The resulting fecal slurry was boiled for 10 min and centrifuged at 20,000×*g* for 10 min at 4 °C, subsequently. The supernatants were collected and measured for inulin concentration by the Fructan Assay Kit (Megazyme, K-FRUC) according to the manufacturer's instructions.

3. Results & discussion

3.1. Properties of mixtures for electrospraying

The mixtures electrosprayed are described in section 2.3. To summarize, the final materials were 3.0 wt% PVA and, separately, 2.5 wt% PVA and 7.5 wt% inulin in H_2O/AA/Ethanol (91/3.4/5.6 by volume). These concentrations and solvents were optimized for MP production rather than beaded fiber or fiber production. The pure inulin suspensions were not electrosprayable; therefore, their properties are not reported. However, Table 1 shows that the addition of inulin to the mixture caused a reduction of conductivity, an increase in viscosity, and a slight reduction of surface tension. A reduction of conductivity with inulin has been previously reported and may be related to interactions between inulin and PVA (Guo et al., 2018). The viscosity increase correlates with increasing overall solid content (Kumar et al., 2014). The slight reduction of surface tension with increasing inulin concentration has also been previously reported (Usman et al., 2021). How these differences in properties may affect the particles produced will be discussed in section 3.2.

Table 1
Conductivity, viscosity, and surface tension of electrosprayed material solutions.

Sample	Conductivity (μS/cm)	Viscosity (cP)	Surface tension (mN/m)
PVA	709 ± 0.7	37.8 ± 2	57.3 ± 0.06
PVA:Inulin	620 ± 1	198 ± 5	52.5 ± 0.04

3.2. Particle size, size distribution, and morphology

The SEM images in Fig. 1 show the as-received inulin and the production of MPs with varying diameters and shapes. It should be noted that the electrospraying conditions were optimized to maximize particle production. We acknowledge that some differences observed from the characterization methods could result because of variability in electrospray conditions. The as-received inulin (Fig. 1(a)) has an average diameter of 9.5 ± 2.7 μm and layered surfaces leading to a less spherical shape. MPs made of PVA (Fig. 1(b)) had an average diameter of 0.35 ± 0.22 μm and were the most spherical. MPs made of 1:3 PVA-inulin (Fig. 1(c)) had an average diameter of 0.42 ± 0.46 μm, respectively, and were more non-spherical than the pure PVA MPs. The presence of inulin in the microparticles correlated with a significant increase in average diameter, as evidenced by the 2-sample *t*-test ($\alpha = 0.05$, $p < 0.001$). However, the PVA-inulin MPs are still an order of magnitude smaller than the as-received inulin.

The particle size dispersity, Cv, is 0.29, 0.63, and 1.10 for the as-received inulin, pure PVA MPs, and PVA-inulin MPs, respectively. The presence of inulin in the MPs is correlated with an increase in size dispersity. This increased MP size dispersity can also be demonstrated by the maximum diameters of MPs. The maximum observed diameter for the PVA-inulin MPs was 5.2 μm, while that of the pure PVA MPs was 2.1 μm.

We hypothesize that the incorporation of inulin generates several effects. First, the PVA-inulin mixtures had a lower conductivity and a higher viscosity than the pure PVA solutions. Both these characteristics can contribute to greater particle sizes and size dispersity (Abyadeh et al., 2017; Felice et al., 2015; Morais et al., 2020). Indeed, we observe such a correlation.

Flow rate is another parameter that can influence particle size and size distribution. Greater flow rates typically result in larger particles and increased size distribution (Alehosseini et al., 2018; Smeets et al., 2017). Although only a modest change (25%), the greater flow rate used for PVA-inulin mixtures (0.5 mL/h) compared to the pure PVA solutions (0.4 mL/h) could also contribute to their greater size distribution.

The PVA MPs made here are about half the average size and 50% more polydisperse than a prior report in the literature (Felice et al., 2015). The operating conditions of the present study relative to the literature study are the following: the flow rate is higher (0.4 mL/h vs 0.3 mL/h or less); the needle diameter is larger (18 gauge vs 24–25 gauge); and, the voltages are higher (21–25 kV compared to ~10 kV). The smaller size is consistent with the larger voltages used in this study. Larger voltages can lead to smaller particles because of the greater strength of the drawing force relative to the surface tension (Alehosseini et al., 2018; Felice et al., 2015). Moreover, the polydispersity has been reported to increase with increased flow rate and increased needle diameter because of the increased presence of multiple jets, yielding multiple particle production sites at the outlet rather than a single site as associated with just one jet (Alehosseini et al., 2018; Cloupeau & Prunet-Foch, 1990; Grace & Marijnissen, 1994; Smeets et al., 2017). High voltages can also lead to broader size distributions because of destabilization of the electrospray jet (Felice et al., 2015).

3.3. Chemical composition by FTIR

As reported in Fig. 2, the FTIR spectrum of inulin shows two peaks at 988 and 933 cm^{-1}. These peaks are associated with the C–C and C–O stretching as well as C–*O*–H and C–*O*–C deformation modes of oligo- and

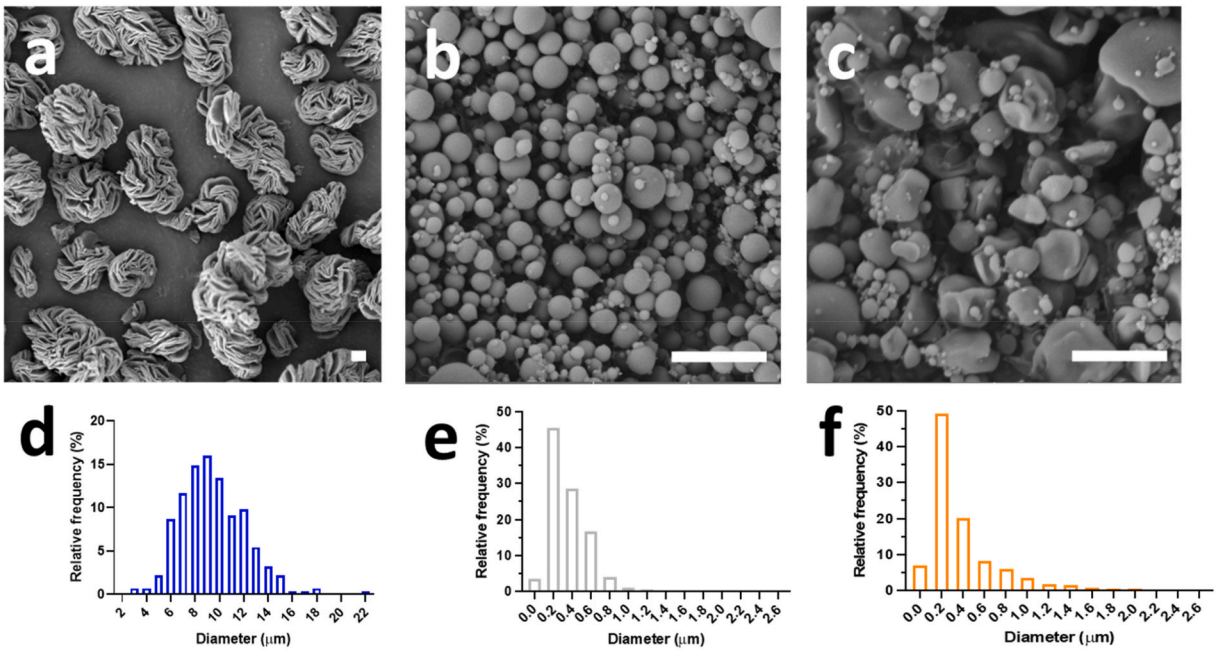

Fig. 1. Scanning Electron Microscopy and size distributions of dry inulin as-received (a & d), electrosprayed MPs made of pure PVA (MW = 89,000–98,000 g/mol) (b & e), and electrosprayed MPs made of PVA (MW = 89,000–98,000 g/mol) and inulin at a ratio of 1:3 (c & f). All micrographs were taken with a voltage of 5.0 kV, a working distance of ~10 mm, beam intensity of 8.00. The scale bars are 2 μm.

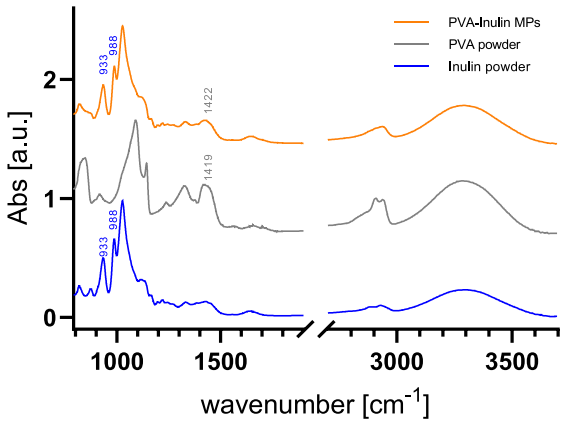

Fig. 2. FTIR spectra for PVA-inulin microparticles compared to their primary components: PVA powder and inulin powder.

polysaccharides, as previously discussed in (Melanie et al., 2015) and (El-Kholy et al., 2020). These peaks are not present in the as received PVA powder but are present in the PVA-inulin MP spectrum, confirming the presence of inulin in the MPs. The spectrum of the PVA powder shows a peak at ~1420, representing O–H bending. This peak is not apparent in the as-received inulin powder but is present in the PVA-inulin MP spectra. These results, therefore, confirm the presence of PVA in the MPs.

3.12 Confocal laser scanning microscopy assesses colocalization of PVA and inulin in the microparticles

PVA/inulin MP size and sphericity, as assessed from confocal microscopy images of the fluorescently labeled MPs (Fig. 3), are similar to the SEM micrographs of Fig. 1. We observed colocalization of PVA (green, Fig. 3a and d) and inulin (red, b and e) within each particle, rather than sequestration of materials into separate particles. When observing a single MP (Fig. 3(d–f)), this colocalization is also apparent. From these confocal microscopy images and FTIR data, we conclude that both inulin and PVA are co-dispersed within the individual particles.

3.4. Microparticle hydration

Confocal microscopy images were acquired to characterize the hydration of the particulate microstructure of inulin, PVA MP, and PVA-inulin MP suspensions (Fig. 4). The duration of the measurements is comparable to the typical GI transit time in mice, as given in the IVIS imaging study below and by (Padmanabhan et al., 2013). The duration is also comparable to the rheological measurements discussed subsequently. The initial few minutes of the time evolution of these concentrated samples could not be captured due to the time to initiate the experiment, which included sample mixing, loading, and sealing of the device. A video of the hydration of the MPs in a dilute case is given in the SI. Although different from the concentrated states in Fig. 4, the video provides insights into these initial few minutes of swelling and aggregation of MPs.

The images in Fig. 4 show the following. For the PVA-inulin MPs (Fig. 4(a)), we observe particle swelling and aggregation as well as some PVA dissolution. In this hydrated state, inulin appears encapsulated by the PVA; the particles are mostly inulin (red) and are dispersed in and around a PVA (green) matrix. The PVA matrix here appears to be partially dissolved and spread throughout the sample in this hydrated state. Furthermore, these swelled, aggregated particles remain stable for longer than 4 h.

The control sample of PVA MPs in Fig. 4(b) shows partial dissolution and swelling. The initially spherical particles (c.f. SEM images of Fig. 1) are no longer distinct. The remaining undissolved PVA remains stable for longer than 4 h. In comparison, the other control, the as-received inulin suspension (Fig. 4(a)), exhibits little to no swelling or aggregation of the inulin particles. Nevertheless, these particles are still slightly larger and more dispersed through the sample than those in PVA-inulin MP suspension. This inulin suspension sample also remains stable for longer than 4 h. It should be noted that the environment of the GI tract could affect the particle hydration process. Oral administration to mice

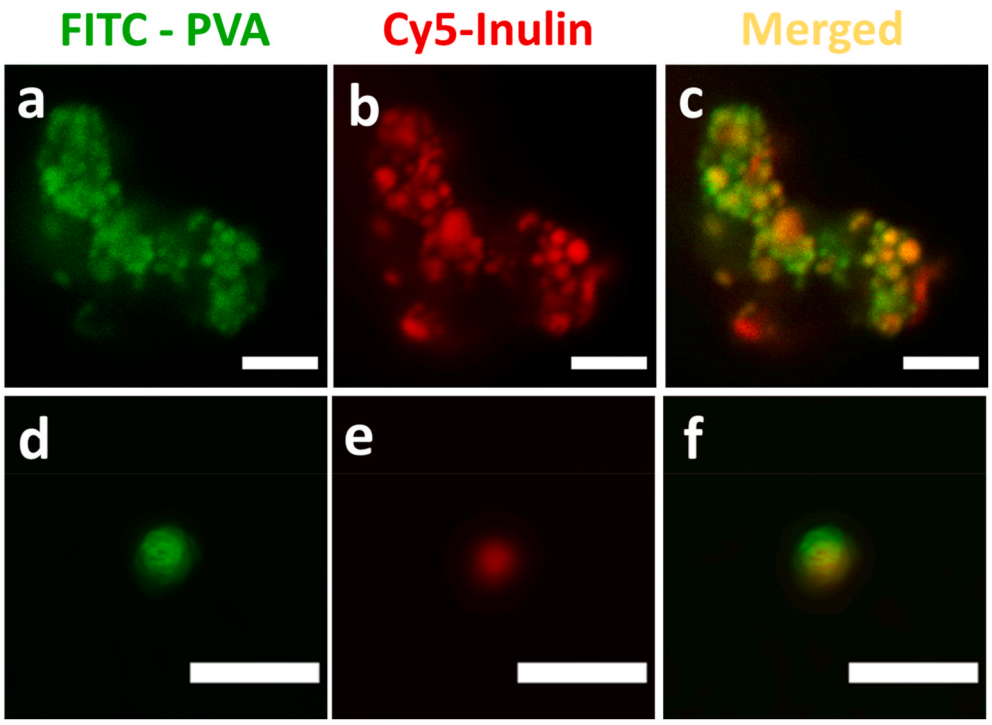

Fig. 3. Confocal laser scanning microscopy images of dry electrosprayed FITC-PVA:Cy5-Inulin MPs. (a) & (d) shows the FITC channel only; (b) & (e) shows the Cy5 channel only; (c) & (f) shows combined FITC and Cy5 channels. The scale bar for (a)–(c) is 5 μm while that of (d)–(f) is 2 μm.

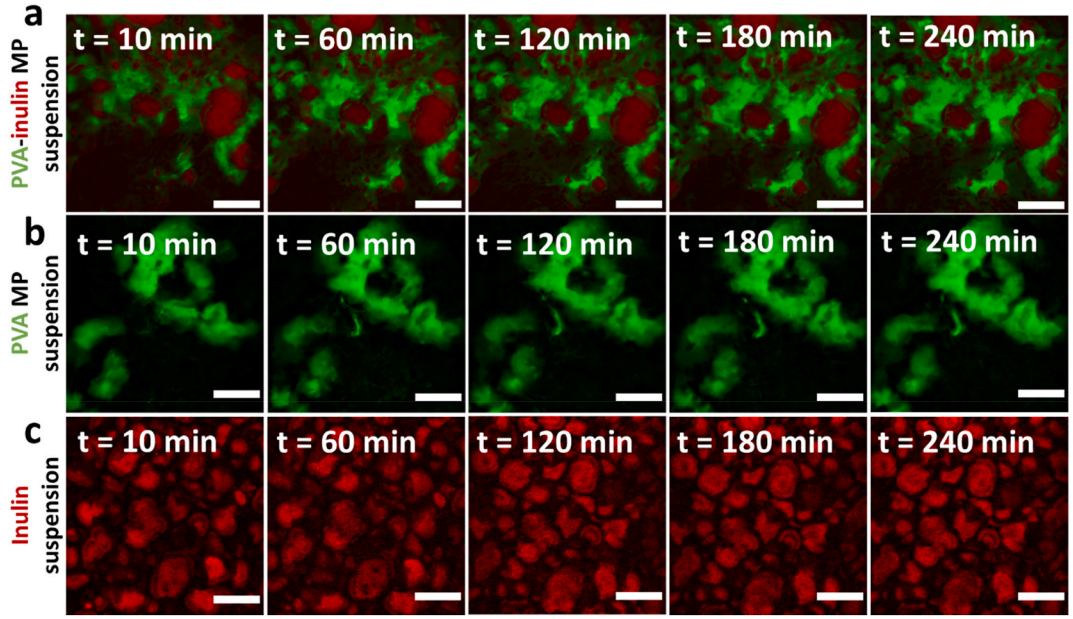

Fig. 4. Confocal laser scanning microscopy images of the time evolution of (a) electrosprayed FITC-PVA:Cy5-Inulin MP suspension, (b) electrosprayed FITC-PVA MP suspension, and (c) FITC-inulin suspension. PVA and inulin are displayed in green and red, respectively. Images were taken at the same location at different times after mixing with water, scale bar = 10 μm.

(described in Section 2.9) occurred through feeding needles which bypassed dilution from saliva, going directly to the stomach. However, as shown in this study, valuable information was still gathered by measuring hydration in water.

It is interesting to compare these measurements to the characterization of the dry MPs as reported in Fig. 1. The colocalized PVA and inulin observed in the dry state become separately sequestered in the hydrated state. Additionally, the MP form of the PVA is no longer observable in the hydrated state. We conclude that the PVA is likely encapsulating the inulin. Furthermore, Fig. 4 suggests that any rheological change in the sample in this timeframe occurs on the molecular or polymeric level because very little microstructural change is visible with confocal microscopy.

The diameter of the PVA and PVA-inulin MPs and the as-received inulin were measured after exposure to water for 30 min under dilute conditions (Fig. 5). Dilute conditions are expected to exaggerate the swelling effects relative to the confocal images shown above due to increased solvation driving force. Under these hydration conditions, an

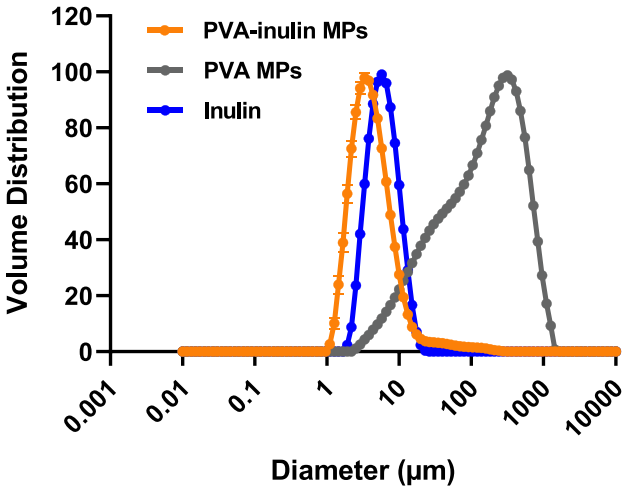

Fig. 5. Size distributions of inulin suspension particles (as received), PVA MPs, and PVA-Inulin MPs in their hydrated state after 30 min of exposure to water in the dilute regime.

increase in particle size is observed for the MPs relative to the dry particle sizes, as reported in Fig. 1. Specifically, the most probable diameter of the PVA MP increases by three orders of magnitude to 316 μm; the most probable diameter of the PVA/inulin MPs increases by one order of magnitude to 3.3 μm. On the other hand, the as-received inulin does not experience a significant change in particle size when hydrated (most probable diameter ~ 7.8 μm). These data confirm the size difference between hydrated inulin and hydrated PVA-inulin MPs observed in the confocal images in Fig. 4.

We thus observe that the particles whose size increases contain PVA. That is, the observed greater swelling for the PVA MPs here and the lack of significant swelling of inulin suggest PVA controls the size change with hydration. This difference in swelling is likely related to the difference in hydrophilicity of the two polymers. PVA is very hydrophilic and will swell more in water (Harpaz et al., 2019) while inulin is known to be more hydrophobic; it will swell less or not at all (Kirtania et al., 2021; Mensink et al., 2015).

MP agglomeration may also contribute to the greater size, as described in other systems (Bchir et al., 2019). Moreover, partially dissolved PVA could contribute to the larger measured sizes of PVA MPs and PVA-inulin MPs. There is some evidence for such partial dissolution in the confocal microscopy images of Fig. 4.

3.5. Rheological characterization of microparticle suspensions

Rheological properties of the PVA/inulin MP suspensions as administered in the *in vivo* studies are compared to that of PVA MP and as received inulin suspensions in Fig. 6. For this study, t = 0 s is after 30 min of incubation in a 37 °C water bath. This incubation time and water bath temperature were used to conform to timing and sample preparation in the mice experiments discussed later.

The duration of the transient measurements shown in (a) is comparable to the typical GI transit time in mice, as given in the IVIS imaging study below and by (Padmanabhan et al., 2013). The linear elastic modulus of the PVA/inulin MP suspension increases by about a factor of ten over the duration of the experiment. The elastic modulus of the inulin suspension control grows over a time comparable to the PVA-inulin MPs; however, the level of increase is much greater; the elastic modulus of this material grows by a factor of about one thousand. In contrast, the PVA MP suspensions have an elastic modulus that is nearly independent of time. Moreover, with time, the elastic modulus of

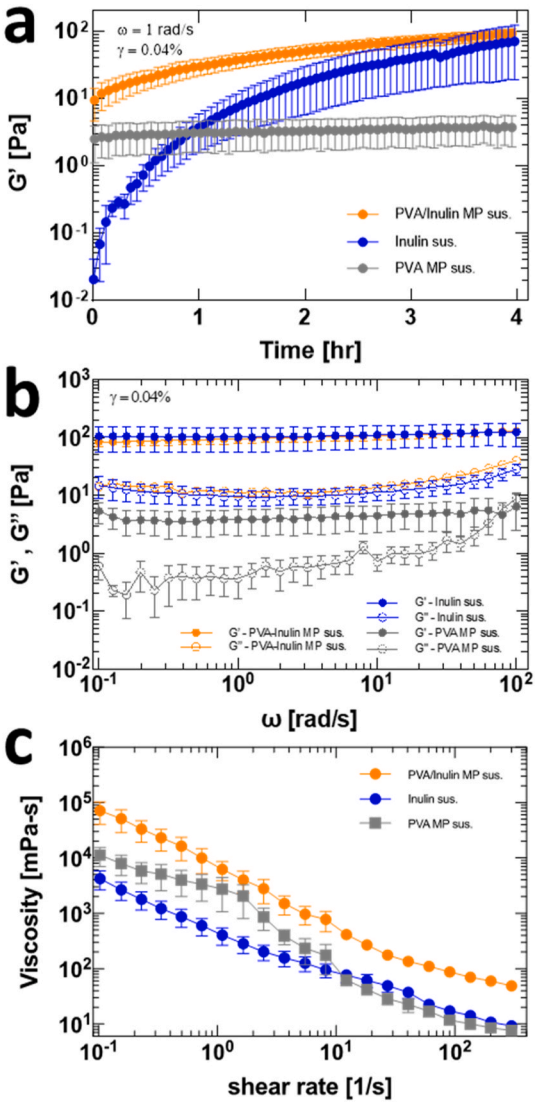

Fig. 6. (a) Time-dependent linear elastic modulus over 4 h ($\gamma = 0.04\%$ and $\omega = 1$ rad/s); (b) frequency-dependent linear viscoelastic moduli (t = 4 h, $\gamma = 0.04\%$); and, (c) shear-rate dependent viscosity (t = 4 h, $\dot{\gamma} = 0.1$ to 300 s-1) of PVA-inulin MP suspensions and pure inulin suspensions.

the PVA-inulin MP suspensions tends towards that of the as-received inulin suspensions rather than that of the PVA MP suspensions.

The frequency-dependent linear viscoelastic moduli reported in Fig. 6(b) were collected at the conclusion of the kinetic measurements reported in Fig. 6(a). The results are consistent with convergent rheological properties of the PVA/inulin MPs and the inulin control. That is, the linear viscoelastic moduli of these two materials are indistinguishable from each other. The moduli of the PVA-MPs are lower than the other two samples.

The shear-rate dependent viscosity of the three specimens shows shear thinning behavior (Fig. 6(c)). There is no evidence of a plateau viscosity at either high or low shear rates. Generally speaking, typical shear rates found in the digestive tract are between 0.1 s^{-1} and 10 s^{-1} (Hardacre et al., 2016; Lentle et al., 2005; Tamargo et al., 2019). The PVA-inulin MP suspensions display the greatest viscosity over the entire range of physiologically relevant shear rates. Inulin suspensions, on average, display the lowest viscosity and pure PVA MP suspensions display viscous properties intermediate between the other two samples. The shear-thinning character of the PVA-inulin MP and inulin control are similar. The PVA MP curve differs in shape from the others; this

material displays two regimes of shear-thinning behavior. It should be noted that this shear-thinning behavior of the inulin suspensions may be related to its observed poor performance in electrospraying on its own. Previous studies have shown that strongly shear thinning polysaccharide solutions usually do not form fibers or particles via electrohydrodynamic processing (Stijnman et al., 2011).

A scenario that explains these data is the following: the elastic modulus is most sensitive to the release and hydration of inulin, while the shear-rate-dependent viscosity is sensitive to both MP form and the presence of inulin. The sensitivity of the elastic modulus to inulin is most apparent from Fig. 6(a), where the pure inulin suspension experiences the greatest modulus increase with time. Furthermore, the convergence of the moduli of the pure inulin suspensions with PVA-inulin MP suspensions suggests that inulin is the common feature that dominates the viscoelastic response.

To investigate this further, we first compared the rheology of PVA-inulin MP suspensions to that of PVA-inulin two-component mixtures (shown in SI Fig. 4). These data show that the PVA-inulin MP suspension initially has a greater modulus than the equivalent two-component mixture. However, with time, these two samples evolve towards the same behavior, which converges to the pure inulin suspension again (Fig. 6(b)).

Next, we evaluate the effect of the MP form alone on rheological behavior by looking at pure PVA solutions and pure PVA MP suspensions. SI Fig. 5 shows that the MP form does indeed cause an increase in the viscoelastic moduli of the PVA in both the transient and frequency-dependent response. However, this modulus remains constant with time and frequency, suggesting that the elastic modulus is not dominated by the MP form. Together, these data indicate that the MP form initially dominates the transient viscoelastic behavior, but this influence lessens with time and a transition occurs to a long-time regime that is dominated by the inulin contribution.

The features that dominate the strain rate dependent viscosity can be similarly evaluated in Fig. 6 and SI Figs. 4 and 5fig4. First, Fig. 6(c) shows that all samples have non-Newtonian shear thinning behavior where the magnitude of the shear-rate dependent viscosity of the PVA-inulin MP suspensions is almost equivalent to the sum of the pure PVA MP and inulin suspensions. These results suggest that both inulin and MP form influence this behavior. Inspecting further, instead of a shear-rate independent viscosity that is typical of PVA solutions (SI Fig. 5), the pure PVA MP suspensions have non-Newtonian shear-thinning behavior. This result suggests that despite the lessening effect on the viscoelastic behavior, the MP form contributes to the shear thinning behavior of the sample. PVA-inulin two-component mixtures and PVA-MP suspensions both show shear thinning behavior. However, PVA-inulin MP suspensions show greater shear thinning. Therefore, inulin affects the strain rate dependent viscosity, but to a lesser extent than the MP form.

Summarizing these rheological results, the rheological response of the PVA-inulin MP suspensions shows the effects of both MP form and the presence of inulin. The inulin was observed to be more influential for the linear viscoelastic behavior at long times. The MP form contributed more to the short-time viscoelastic behavior as well as the increased viscosity and shear thinning behavior. Interestingly, all inulin-containing suspensions show rheological change over the 4-h measurement; however, none of the suspensions show visual changes via CLSM in this time period. At the same time, the many small particles observed in the dry state by SEM are not found in the hydrated state. The hydrated size distributions (Fig. 5) confirm the lack of these smaller particles suggesting that they are likely dissolved. Because only the inulin-containing samples show increased elastic modulus with time and inulin suspensions themselves are visually observed to gel over 4 h, we hypothesize that the presence and interactions of dissolved inulin are responsible for the observed rheological changes.

3.6. Inulin release profile

The inulin release profile in the simulated intestinal fluid (SIF) of the PVA-inulin MPs is compared to inulin as-received in Fig. 7. This figure indicates that the MPs follow a burst release profile of inulin. More specifically, in the first 2 h, ~70% of inulin is released from the PVA-inulin MP suspensions. Additionally, the PVA-inulin MP suspensions attain steady-state after approximately 500 min. Even though this *in vitro* assay is expected to display a faster release of inulin than the rheological experiments (Fig. 6) because of the different environments (diluted in SIF compared to the constant concentration in DI water, respectively), the release profile shows a time scale that is comparable to the kinetics in the transient rheological response of Fig. 6(a). This correspondence further supports the hypothesis that the release of inulin impacts the kinetics of the transient rheological response of the PVA-inulin MP suspension.

3.7. Gut retention study

Retention of inulin in the gastrointestinal tracts of mice was first evaluated by live animal imaging. Cyanine 7-conjugated inulin was added to the PVA-inulin MPs, PVA-inulin mixture, and inulin as-received in the 1:19 ratio to native inulin. Then the fluorescence-labeled formulations were fed to mice via oral gavage. Extended gut retention was not identified in the mouse live imaging results (SI Fig. 7) because the method cannot differentiate the various segments of the GI tract when the stomach and intestines are naturally arranged in mice. To accurately capture the difference in colon retention, fecal samples were instead collected and imaged to measure the Cy7-inulin signal (Fig. 8). The onset of inulin excretion was at 5.0 h for most mice. This suggests an overall GI transit time of 5 h, consistent with the literature (Padmanabhan et al., 2013). The fluorescent intensity reached the peak at 10 h for the inulin and PVA-inulin mixture. In comparison, the maximum signal for the PVA-inulin MPs was seen after 15 h (Fig. 8(b)). This significant delay indicates that the inulin microparticles traverse the GI tract more slowly than both the free inulin and PVA-inulin mixtures. This difference could improve the availability of inulin for gut-residing microbes.

In order to confirm the prolonged colon retention of MPs, the inulin excretion kinetics in the feces was also evaluated, shown in Fig. 9. The inulin content measured the total amount of long-chain inulin remaining in the feces, which excludes degraded fructose from inulin. We first note that the as-received inulin and PVA-inulin mixture reached the highest

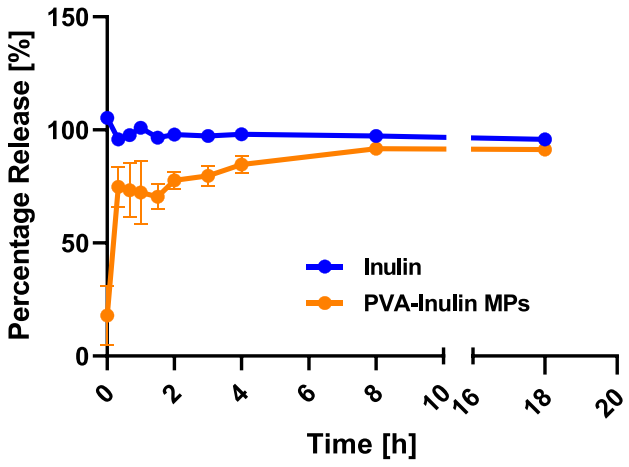

Fig. 7. Release profile of inulin from the microparticles compared to as received inulin.

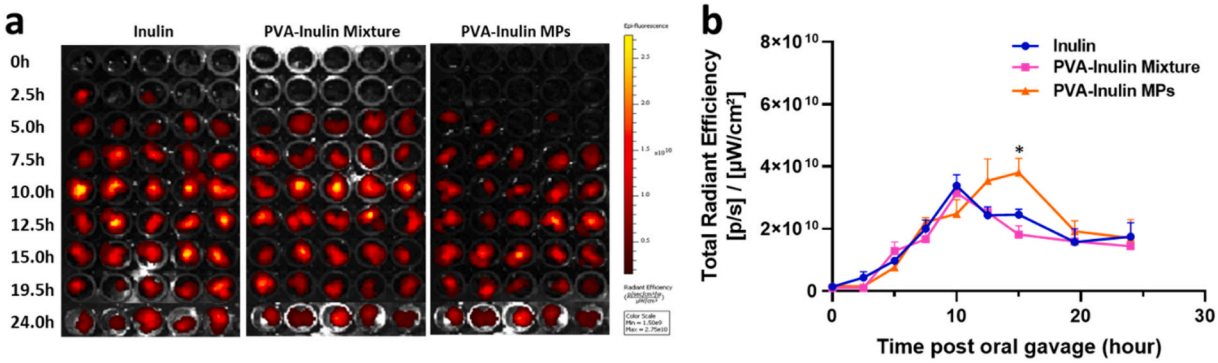

Fig. 8. Gut retention study of PVA-inulin MPs by fecal excretion. Mice were orally gavaged with Cy7-labeled inulin, PVA-Cy7-Inulin mixture, or Cy7-MPs, and fecal samples were collected at indicated time points (a) Images of fecal pellets collected and (b) total fluorescence intensity of the feces, quantified from (N = 5).

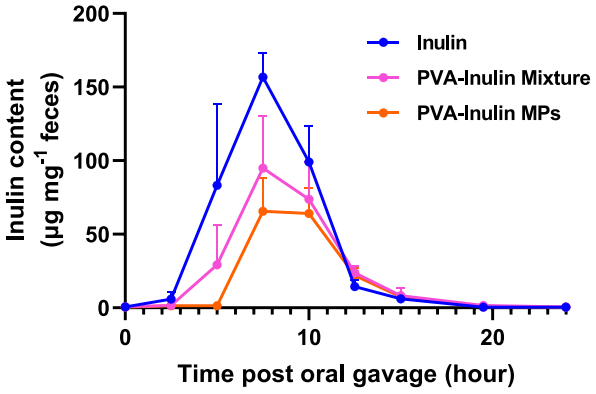

Fig. 9. Fecal inulin content of mice over 24 h after oral administration of as-received inulin, PVA-inulin mixture, and PVA-inulin MPs.

fecal concentration by ~7.5 h, while the PVA-inulin MPs reached their maximum by around 10 h. This delayed peak for the PVA-inulin MPS further supports the enhanced colon retention of the microparticle form of inulin. These data also show a reduction of the total amount of inulin present in the feces for the PVA-inulin mixture and PVA-inulin MPs - the greatest reduction for the MPs. This reduction can be explained by the inulin assay kit and the fact that it only measures long-chain inulin remaining in the feces. Colon fermentation is expected to break down the polysaccharide and generate fructose from inulin, therefore reducing the amount of long-chain inulin present (Flint et al., 2012). Consequently, the lower inulin content detected in the fecal samples from the PVA-inulin mixture and MPs treated mice can be attributed to the extended transit times, which allow for more fermentation.

Comparing the feces quantification from these two different methods (Figs. 8 and 9) identifies similarities and differences. Both quantifications show a later appearance of peak inulin content for the MPs, suggesting enhanced colon retention. However, there is an approximate 2.5 h delay in the transit time in the live animal imaging (SI Fig. 7(b)) compared to the direct measurement of inulin (Fig. 9). This delay may be ascribed to the frequent anesthesia performed in mice when acquiring the live images. It has been reported that inhalation anesthesia may disrupt normal gastrointestinal motility (Dryn et al., 2018; Flint et al., 2012). Additionally, the reduction of inulin content for the PVA-inulin mixture and MPs in Fig. 9 suggests more of the inulin in these samples is fermented, consistent with enhanced colon retention. This reduction is not observed from the fluorescence quantification in Fig. 8, where the fluorophore persists even when the conjugated inulin is degraded.

These results can be explained by the mucoadhesive properties of the highly hydrolyzed PVA (Popov et al., 2016; Suchaoin et al., 2016) and the increased viscosity/moduli of the sample described in section 3.6 and SI. Essentially, these two features of the MP suspensions could contribute to an increase in bioavailability of the inulin fermentation by colon residing bacteria (Fig. 9). The gut retention trends of these three samples align with the trends in viscosity at the physiological shear rates (0.1 s^{-1} and 10 s^{-1}) (Hardacre et al., 2016; Lentle et al., 2005; Tamargo et al., 2019). Specifically, the greatest gut retention of inulin, as quantified here, occurred with the sample with the greatest viscosity at shear rates = 0.1 s^{-1} - 10 s^{-1} (PVA-inulin MP suspension); the least gut retention of inulin occurred with the sample with the lowest viscosity in this regime (inulin suspension). A direct comparison of these samples is given in the SI. Further animal studies could investigate the gut microbiome composition and changes in metabolite levels, such as SCFAs. Such measurements would provide greater insight into specific prebiotic effects of modified inulin. Nonetheless, colon-targeting and retentive formulation are promising strategies for modulating host microbiome in multiple diseases applications.

4. Conclusions

In conclusion, inulin was successfully electrosprayed into microparticles by blending it with a PVA solution at a ratio of 1:3 PVA-inulin by weight. The MP form and presence of inulin had significant effects on transient, hydration-induced rheological properties when suspended in water. The rheological differences between samples were observed in both linear viscoelastic modulus and steady shear viscosity measurements: inulin-containing samples had greater viscoelastic moduli and shear-rate dependent viscosity. When administered to mice and compared to inulin as-received and PVA-inulin mixtures, PVA-inulin MP suspensions resulted in greater colon retention as given by fecal quantification and IVIS imaging. We conclude that this response is correlated with the modified rheological properties of the microparticle hydration and the mucoadhesive properties of the PVA incorporated into the formulation. These results expand our understanding of the effect of inulin formulation and rheological properties on the prebiotic effect of inulin. They can be helpful in the design of colon-targeted products in both food and biomedical applications, especially for gut microbiome modulation through prebiotics.

Author statement

Keara T. Saud:Conceptualization, Investigation, Formal analysis, Writing - Original Draft, Jin Xu:Conceptualization, Investigation, Formal analysis, Writing - Review & Editing, Sabina Wilkanowicz: Methodology, Investigation, Writing - Review & Editing, Yue He: Investigation, James J. Moon:Writing - Review & Editing, Funding acquisition, Michael J. Solomon:Supervision, Writing - Review & Editing, Funding acquisition.

Declaration of competing interest

The authors declare the following financial interests/personal relationships which may be considered as potential competing interests: James J. Moon reports a relationship with EVOQ Therapeutics, Saros Therapeutics, and Intrinsic Medicine that includes: board membership, consulting or advisory, equity or stocks, and funding grants. James J. Moon and Jin Xu has patent pending to University of Michigan, Ann Arbor.

Data availability

Data will be made available on request.

Acknowledgements

The authors acknowledge a Rackham Research grant and NIH (R01DK125087, R01CA271799) for financial support. We also acknowledge the Michigan Center for Materials Characterization and Van Vlack lab for the use of the instruments and staff assistance. The authors would like to also acknowledge Angelica Rose Galvan for helpful discussions and preliminary work and Taylor Repetto for her assistance in the surface tension measurements.

Appendix A. Supplementary data

Supplementary data to this article can be found online at https://doi.org/10.1016/j.foodhyd.2023.108625.

References

Abyadeh, M., Karimi Zarchi, A. A., Faramarzi, M. A., & Amani, A. (2017). Evaluation of factors affecting size and size distribution of chitosan-electrosprayed nanoparticles. *Avicenna Journal of Medical Biotechnology, 9*, 126.

Afinjuomo, F., Abdella, S., Youssef, S. H., Song, Y., & Garg, S. (2021). Inulin and its application in drug delivery. *Pharmaceuticals, 14*. https://doi.org/10.3390/PH14090855

Alehosseini, A., Ghorani, B., Sarabi-Jamab, M., & Tucker, N. (2018). Principles of electrospraying: A new approach in protection of bioactive compounds in foods. *Critical Reviews in Food Science and Nutrition*. https://doi.org/10.1080/10408398.2017.1323723

Barclay, T., Ginic-Markovic, M., Cooper, P., & Petrovsky, N. (2010). Inulin - a versatile polysaccharide with multiple pharmaceutical and food chemical uses. *The Journal of Excipients and Food Chemicals, 1*, 27–50.

Bchir, B., Sadin, N., Ronkart, S. N., & Blecker, C. (2019). Effect of powder properties on the physicochemical and rheological characteristics of gelation inulin–water systems. *Colloid & Polymer Science, 297*, 849–860. https://doi.org/10.1007/s00396-019-04510-9

Beirão-da-Costa, S., Duarte, C., Bourbon, A. I., Pinheiro, A. C., Januário, M. I. N., Vicente, A. A., Beirão-da-Costa, M. L., & Delgadillo, I. (2013). Inulin potential for encapsulation and controlled delivery of Oregano essential oil. *Food Hydrocolloids, 33*, 199–206. https://doi.org/10.1016/j.foodhyd.2013.03.009

Carlson, J. L., Erickson, J. M., Lloyd, B. B., & Slavin, J. L. (2018). Health effects and sources of prebiotic dietary fiber. *Current Developments in Nutrition*. https://doi.org/10.1093/cdn/nzy005

Cloupeau, M., & Prunet-Foch, B. (1990). Electrostatic spraying of liquids: Main functioning modes. *Journal of Electrostatics, 25*, 165–184. https://doi.org/10.1016/0304-3886(90)90025-Q

Dryn, D., Luo, J., Melnyk, M., Zholos, A., & Hu, H. (2018). Inhalation anaesthetic isoflurane inhibits the muscarinic cation current and carbachol-induced gastrointestinal smooth muscle contractions. *European Journal of Pharmacology, 820*, 39–44. https://doi.org/10.1016/J.EJPHAR.2017.11.044

El-Kholy, W. M., Aamer, R. A., & Ali, A. N. A. (2020). Utilization of inulin extracted from chicory (Cichorium intybus L.) roots to improve the properties of low-fat synbiotic yoghurt. *Annals of Agricultural Science, 65*, 59–67. https://doi.org/10.1016/J.AOAS.2020.02.002

Felice, B., Prabhakaran, M. P., Zamani, M., Rodríguez, A. P., & Ramakrishna, S. (2015). Electrosprayed poly(vinyl alcohol) particles: Preparation and evaluation of their drug release profile. *Polymer International, 64*, 1722–1732. https://doi.org/10.1002/pi.4972

Flint, H. J., Scott, K. P., Duncan, S. H., Louis, P., & Forano, E. (2012). Microbial degradation of complex carbohydrates in the gut. *Gut Microbes*. https://doi.org/10.4161/gmic.19897

Ghorani, B., & Tucker, N. (2015). Fundamentals of electrospinning as a novel delivery vehicle for bioactive compounds in food nanotechnology. *Food Hydrocolloids*. https://doi.org/10.1016/j.foodhyd.2015.05.024

Grace, J. M., & Marijnissen, J. C. M. (1994). A review of liquid atomization by electrical means. *Journal of Aerosol Science, 25*, 1005–1019. https://doi.org/10.1016/0021-8502(94)90198-8

Guo, M., Wang, H., & Wang, C. (2018). Interactions between whey protein and inulin in a model system. *Journal of Food Science & Technology, 55*, 4051. https://doi.org/10.1007/S13197-018-3331-7

Han, K., Nam, J., Xu, J., Sun, X., Huang, X., Animasahun, O., Achreja, A., Jeon, J. H., Pursley, B., Kamada, N., Chen, G. Y., Nagrath, D., & Moon, J. J. (2021). Generation of systemic antitumour immunity via the in situ modulation of the gut microbiome by an orally administered inulin gel. *Nature Biomedicine Engineering, 5*, 1377–1388. https://doi.org/10.1038/s41551-021-00749-2

Hardacre, A. K., Lentle, R. G., Yap, S. Y., & Monro, J. A. (2016). Does viscosity or structure govern the rate at which starch granules are digested? *Carbohydrate Polymers, 136*, 667–675. https://doi.org/10.1016/j.carbpol.2015.08.060

Harpaz, D., Axelrod, T., Yitian, A. L., Eltzov, E., Marks, R. S., & Tok, A. I. Y. (2019). Dissolvable polyvinyl-alcohol film, a time-barrier to modulate sample flow in a 3D-printed holder for capillary flow paper diagnostics. *Materials, 12*. https://doi.org/10.3390/MA12030343

Hauser-Kawaguchi, A., Milne, M., Li, F., Lee, T. Y., & Luyt, L. G. (2019). The development of a near infrared inulin optical probe for measuring glomerular filtration rate. *International Journal of Biological Macromolecules, 123*, 255–260. https://doi.org/10.1016/J.IJBIOMAC.2018.11.034

Jacobsen, C., García-Moreno, P. J., Mendes, A. C., Mateiu, R. V., & Chronakis, I. S. (2018). Use of electrohydrodynamic processing for encapsulation of sensitive bioactive compounds and applications in food. *Annual Review of Food Science and Technology, 9*, 525–549. https://doi.org/10.1146/annurev-food-030117-012348

Jain, A. K., Sood, V., Bora, M., Vasita, R., & Katti, D. S. (2014). Electrosprayed inulin microparticles for microbiota triggered targeting of colon. *Carbohydrate Polymers, 112*, 225–234. https://doi.org/10.1016/j.carbpol.2014.05.087

Kaneo, Y., Hashihama, S., Kakinoki, A., Tanaka, T., Nakano, T., & Ikeda, Y. (2005). Pharmacokinetics and biodisposition of poly(vinyl alcohol) in rats and mice. *Drug Metabolism and Pharmacokinetics, 20*, 435–442. https://doi.org/10.2133/DMPK.20.435

Kim, H. S., Kim, K. J., Lee, M. W., Lee, S. Y., Yun, Y. H., Shim, W. G., & Yoon, S. D. (2020). Preparation and release properties of arbutin imprinted inulin/polyvinyl alcohol biomaterials. *International Journal of Biological Macromolecules, 161*, 763–770. https://doi.org/10.1016/J.IJBIOMAC.2020.06.105

Kirtania, M. D., Kahali, N., & Maity, A. (2021). Inulin-based hydrogel. In T. K. Giri, & B. Ghosh (Eds.), *Plant and algal hydrogels for drug delivery and regenerative medicine* (pp. 261–292). Elsevier. https://doi.org/10.1016/B978-0-12-821649-1.00005-2.

Kolida, S., Tuohy, K., & Gibson, G. R. (2002). Prebiotic effects of inulin and oligofructose. *British Journal of Nutrition, 87*, S193–S197. https://doi.org/10.1079/BJN/2002537

Kumar, R., Manjunatha, S., Kathiravan, T., Vijayalakshmi, S., Nadanasabapathi, S., & Raju, P. S. (2014). *Rheological characteristics of inulin solution at low concentrations: Effect of temperature and solid content*. https://doi.org/10.1007/s13197-014-1671-5

Lentle, R. G., Hemar, Y., Hall, C. E., & Stafford, K. J. (2005). Periodic fluid extrusion and models of digesta mixing in the intestine of a herbivore, the common brushtail possum (Trichosurus vulpecula). *Journal of Comparative Physiology B: Biochemical, Systemic, and Environmental Physiology, 175*, 337–347. https://doi.org/10.1007/s00360-005-0490-4

Librán, C. M., Castro, S., & Lagaron, J. M. (2017). Encapsulation by electrospray coating atomization of probiotic strains. *Innovative Food Science & Emerging Technologies, 39*, 216–222. https://doi.org/10.1016/j.ifset.2016.12.013

Liu, Y., Leng, Y., Xiao, S., Zhang, Y., Ding, W., Ding, B., Wu, Y., Wang, X., & Fu, Y. (2022). Effect of inulin with different degrees of polymerization on dough rheology, gelatinization, texture and protein composition properties of extruded flour products. *Lebensmittel-Wissenschaft und -Technologie, 159*, Article 113225. https://doi.org/10.1016/j.lwt.2022.113225

Melanie, H., Susilowati, A., Iskandar, Y. M., Lotulung, P. D., & Andayani, D. G. S. (2015). Characterization of inulin from local red dahlia (dahlia sp. L) tubers by infrared spectroscopy. *Procedia Chemistry, 16*, 78–84. https://doi.org/10.1016/j.proche.2015.12.027

Mensink, M. A., Frijlink, H. W., Van Der Voort Maarschalk, K., & Hinrichs, W. L. J. (2015). Inulin, a flexible oligosaccharide I: Review of its physicochemical characteristics. *Carbohydrate Polymers*. https://doi.org/10.1016/j.carbpol.2015.05.026

Morais, A.Í. S., Vieira, E. G., Afewerki, S., Sousa, R. B., Honorio, L. M. C., Cambrussi, A. N. C. O., Santos, J. A., Bezerra, R. D. S., Furtini, J. A. O., Silva-Filho, E. C., Webster, T. J., & Lobo, A. O. (2020). Fabrication of polymeric microparticles by electrospray: The impact of experimental parameters. *Journal of Functional Biomaterials*. https://doi.org/10.3390/jfb11010004

Nieto-Nieto, T. V., Wang, Y. X., Ozimek, L., & Chen, L. (2015). Inulin at low concentrations significantly improves the gelling properties of oat protein - a molecular mechanism study. *Food Hydrocolloids, 50*, 116–127. https://doi.org/10.1016/j.foodhyd.2015.03.031

Oguz, S., Tam, N., Aydogdu, A., Sumnu, G., & Sahin, S. (2018). Development of novel pea flour-based nanofibres by electrospinning method. *International Journal of Food Science and Technology, 53*, 1269–1277. https://doi.org/10.1111/ijfs.13707

Padmanabhan, P., Grosse, J., Asad, A. B. M. A., Radda, G. K., & Golay, X. (2013). Gastrointestinal transit measurements in mice with 99mTc-DTPA-labeled activated charcoal using NanoSPECT-CT. *EJNMMI Research, 3*, 60. https://doi.org/10.1186/2191-219X-3-60

Perez-Masia, R., Lagaron, J. M., & Lopez-Rubio, A. (2014). Surfactant-aided electrospraying of low molecular weight carbohydrate polymers from aqueous solutions. *Carbohydrate Polymers, 101*, 249–255. https://doi.org/10.1016/j.carbpol.2013.09.032

Popov, A., Enlow, E., Bourassa, J., & Chen, H. (2016). Mucus-penetrating nanoparticles made with "mucoadhesive" poly(vinyl alcohol). *Nanotechnology Biology Medicine, 12*, 1863–1871. https://doi.org/10.1016/j.nano.2016.04.006

Rostami, M. R., Yousefi, M., Khezerlou, A., Aman Mohammadi, M., & Jafari, S. M. (2019). Application of different biopolymers for nanoencapsulation of antioxidants via electrohydrodynamic processes. *Food Hydrocolloids*. https://doi.org/10.1016/j.foodhyd.2019.06.015

Sarkar, A., Ademuyiwa, V., Stubley, S., Esa, N. H., Goycoolea, F. M., Qin, X., Gonzalez, F., & Olvera, C. (2018). Pickering emulsions co-stabilized by composite protein/polysaccharide particle-particle interfaces: Impact on in vitro gastric stability. *Food Hydrocolloids, 84*, 282–291. https://doi.org/10.1016/j.foodhyd.2018.06.019

Smeets, A., Clasen, C., & Van den Mooter, G. (2017). Electrospraying of polymer solutions: Study of formulation and process parameters. *European Journal of Pharmaceutics and Biopharmaceutics, 119*, 114–124. https://doi.org/10.1016/j.ejpb.2017.06.010

Stijnman, A. C., Bodnar, I., & Hans Tromp, R. (2011). Electrospinning of food-grade polysaccharides. *Food Hydrocolloids, 25*, 1393–1398. https://doi.org/10.1016/j.foodhyd.2011.01.005

Suchaoin, W., Pereira De Sousa, I., Netsomboon, K., Rohrer, J., Hoffmann Abad, P., Laffleur, F., Matuszczak, B., & Bernkop-Schnürch, A. (2016). Mucoadhesive polymers: Synthesis and in vitro characterization of thiolated poly(vinyl alcohol). *International Journal of Pharmacy, 503*, 141–149. https://doi.org/10.1016/j.ijpharm.2016.03.006

Tamargo, A., Cueva, C., Alvarez, M. D., Herranz, B., Moreno-Arribas, M. V., & Laguna, L. (2019). Physical effects of dietary fibre on simulated luminal flow, studied by in vitro dynamic gastrointestinal digestion and fermentation. *Food & Function, 10*, 3452–3465. https://doi.org/10.1039/C9FO00485H

Usman, M., Zhang, C., Patil, P. J., Mehmood, A., Li, X., Bilal, M., Haider, J., & Ahmad, S. (2021). Potential applications of hydrophobically modified inulin as an active ingredient in functional foods and drugs - a review. *Carbohydrate Polymers, 252*, Article 117176. https://doi.org/10.1016/J.CARBPOL.2020.117176

Van De Wiele, T., Boon, N., Possemiers, S., Jacobs, H., & Verstraete, W. (2007). Inulin-type fructans of longer degree of polymerization exert more pronounced in vitro prebiotic effects. *Journal of Applied Microbiology, 102*, 452–460. https://doi.org/10.1111/j.1365-2672.2006.03084.x

Wahbi, W., Siam, R., Kegere, J., El-Mehalmey, W. A., & Mamdouh, W. (2020). Novel inulin electrospun composite nanofibers: Prebiotic and antibacterial activities. *ACS Omega, 5*, 3015. https://doi.org/10.1021/acsomega.9b03957

Youn, H. G., Je, J. Y., Lee, C. M., & Yoon, S. D. (2019). Inulin/PVA biomaterials using thiamine as an alternative plasticizer. *Carbohydrate Polymers, 220*, 86–94. https://doi.org/10.1016/J.CARBPOL.2019.05.056

Zaeim, D., Sarabi-Jamab, M., Ghorani, B., & Kadkhodaee, R. (2019). Double layer co-encapsulation of probiotics and prebiotics by electro-hydrodynamic atomization. *Lebensmittel-Wissenschaft und -Technologie, 110*, 102–109. https://doi.org/10.1016/j.lwt.2019.04.040

Zaeim, D., Sarabi-Jamab, M., Ghorani, B., Kadkhodaee, R., Liu, W., & Tromp, R. H. (2020). Microencapsulation of probiotics in multi-polysaccharide microcapsules by electro-hydrodynamic atomization and incorporation into ice-cream formulation. *Food Structure, 25*. https://doi.org/10.1016/j.foostr.2020.100147

Zhang, L., Wang, X., Li, S., Sun, J., & Liu, X. (2019). Effect of inulin on the pasting, textural, and rheological properties of sweet potato starch. *CyTA - Journal of Food, 17*, 733–743. https://doi.org/10.1080/19476337.2019.1645738